Optics Letters

Photorefraction-induced Bragg scattering in cryogenic lithium niobate ring resonators

Yuntao Xu,[1] Ayed Al Sayem,[1] Chang-Ling Zou,[1] Linran Fan,[2] Risheng Cheng,[1] and Hong X. Tang[1,*]

[1]Department of Electrical Engineering, Yale University, New Haven, Connecticut 06520, USA
[2]James C. Wyant College of Optical Sciences, University of Arizona, Tucson, Arizona 85721, USA
*Corresponding author: hong.tang@yale.edu

Received 12 November 2020; revised 6 December 2020; accepted 22 December 2020; posted 22 December 2020 (Doc. ID 414702); published 15 January 2021

We report intracavity Bragg scattering induced by the photorefractive (PR) effect in high-Q lithium niobate ring resonators at cryogenic temperatures. We show that when a cavity mode is strongly excited, the PR effect imprints a long-lived periodic space-charge field. This residual field in turn creates a refractive index modulation pattern that dramatically enhances the back scattering of an incoming probe light, and results in selective and reconfigurable mode splittings. This PR-induced Bragg scattering effect, despite being undesired for many applications, could be utilized to enable optically programmable photonic components.

https://doi.org/10.1364/OL.414702

Lithium niobate (LN), as one of the most widely studied optical materials, has played a significant role in nonlinear optics [1] for its rich and favorable optical properties [2]. One unique characteristic of LN is the photorefractive (PR) effect, which arises as a combination of the photo-excited space-charge field and subsequent electro-optic effect, inducing a refractive index variation during light illumination [2,3]. In the past decades, a vast amount of research has been performed to study and control this important feature of LN crystals [4–6]. On one hand, the PR effect is considered to be responsible for optical damage [5], introducing instability and limiting the power handling capability of devices [6,7]. On the other hand, the PR effect could also be utilized for optical holography and storage [8,9].

With the recent development of a smart-cut wafer-bonding technique [10], high-quality thin film single-crystalline LN on insulator (LNOI) has enabled on-chip high-quality-factor (Q) LN resonators [11] and provided a promising chip-scale system for various nonlinear optics applications [7,12–15]. Due to the narrow linewidth of the resonances, LN high-Q microresonators also offer an opportunity to study the refractive index variation induced by the PR effect. The enhanced intracavity optical intensity significantly boosts the PR effect and leads to observations of novel phenomena such as photon-level tuning of resonances and quenching of the PR effect [16–19].

In this Letter, we describe strong Bragg scattering induced by the PR effect in high-Q LN ring resonators measured at 1.8 K. Cryogenic operation of LN microring resonators is critical for exploitation of the strong Pockels nonlinearity of LN for microwave-to-optical photon conversions [20–22] and cryogenic-to-room-temperature data links [23]. As the temperature decreases, the relaxation time of the PR effect increases from tens of milliseconds at room temperature [16,17] to several days at 1.8 K [4]. Thus, the PR-effect-induced electric field can semi-permanently modulate the refractive index of a ring cavity. In particular, a periodic refractive index pattern similar to a Bragg-grating reflector can be built up when launching a strong optical standing wave into selected modes of the cavity. Subsequently, when probed with a weak light, the microring exhibits mode splitting at phase matched wavelengths. An illustration of such a mechanism is shown in Fig. 1. A non-universal mode splitting of cavity resonances has been reported in optical resonators with fine lithographically engineered cavities [24]. Here we achieved selective mode splitting with all-optical control. Moreover, by strongly exciting other cavity modes, the

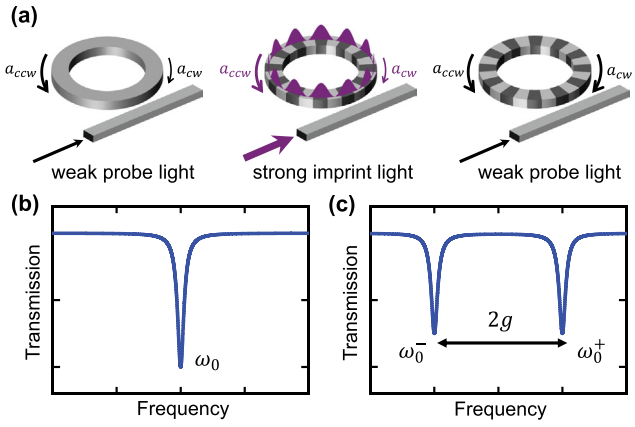

Fig. 1. Optical mode splitting induced by photorefractive effect. (a) When strong light is launched to excite a LN ring cavity, an index pattern is imprinted in the microring by the standing-wave component of light intensity due to the PR effect. The periodic index pattern leads to an enhancement of back scattering in the cavity. (b), (c) Simulated spectrum of a resonance (b) before and (c) after index pattern generation. A mode splitting of $2g$ is generated due to strong coupling between CW mode (a_{cw}) and CCW mode (a_{ccw}), where g is the mode coupling strength.

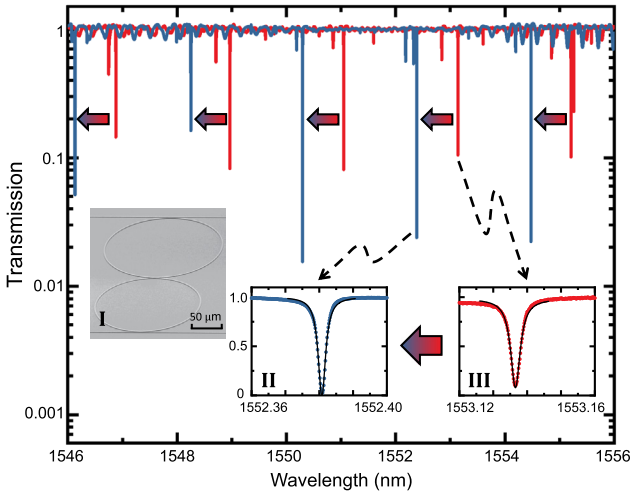

Fig. 2. Long-lived blue resonance shifts occur after periodic laser scanning across the transmission window of the grating couplers. Inset I shows a SEM image of the resonator. Insets II and III show the zoomed-in spectrum of a TE00 mode after and before the periodic scanning, respectively.

imprinted index pattern could be redistributed, thus reconfiguring the mode splitting to other wavelengths. These interesting observations suggest potential exploitation of the PR effect for on-chip all-optically controlled photonic components.

The device used in this work is a high-Q LN coupled double-ring resonator (inset I in Fig. 2) fabricated from a 600 nm x-cut thin-film LNOI wafer (from NANOLN), originally designed for microwave-to-optics conversion [20–22]. The coupled optical ring resonator has a width of 1.6 μm, with radii 80 and 90 μm, respectively, and a coupling gap of 0.7 μm. The device is patterned by electron beam lithography, with 350-nm-thick LN etched through Ar^+-based reactive ion etching. The detailed fabrication process can be found in our previous work [25]. In the final step, the device is coated with 1.5 μm silicon dioxide using plasma enhanced chemical vapor deposition.

In this double-ring device, when the wavelengths of the modes in two rings are close enough, the resonators are strongly coupled and support symmetric and anti-symmetric supermodes [20]. With optical power distributed in both rings, the two supermodes can be probed by a waveguide coupled to one of the rings. Although the specific device we employ here is more complex than a single microring, the impact of the PR effect and the underlying dynamics we elucidate here should apply to a range of other device geometries including simpler ring, racetrack, or disk resonators.

The chip is mounted on a set of attocube stages inside a closed-cycle cryostat and cooled down to 1.8 K. The light output from a tunable laser diode (Santec-710) is sent to a variable optical attenuator (VOA) followed by a polarization controller, then launched into the fridge via a standard single-mode fiber. The light is coupled in and out from the on-chip waveguides through a pair of grating couplers designed to transmit TE polarized light. The light in the 0.8 μm waveguide is coupled to the ring of 80 μm radius with a coupling gap of 1.0 μm. The insertion loss of the chip as well as the fiber inside the fridge is 23 dB, and the output light is detected by a fiber-optic receiver.

The PR effect in LN is an action of several cascaded processes that induce a refractive index variation of the material in the presence of light illumination [3]. Due to the broken inversion symmetry of its crystal structure, when LN is illuminated, a photocurrent is generated along crystalline z direction through the bulk photovoltaic effect. The migrated photo-induced charges are then trapped in defects of crystal, building up a space-charge field opposite to the direction of the photocurrent. The electric field subsequently modulates the refractive index of the LN crystal through the Pockels effect. Specific to the fabricated LNOI microcavities discussed here, the drop in refractive index results in a blue shift of resonance frequency with a relaxation time ranging from tens of milliseconds to several seconds at room temperature [16,17].

The relaxation time of the PR effect rises sharply when the device is cooled down to 1.8 K [3,4]. As the cavity is illuminated at a cryogenic temperature, the space-charge field induced by the PR effect accumulates and leads to long-lived modulation of resonances in the cavity. A continuous blue shift of all resonances is observed when we repeatedly scan the laser from 1500 to 1600 nm within the transmission window of the grating couplers with an input power of 5 dBm into to the fridge (−6.5 dBm on the input waveguide). The blue shift of resonance reaches saturation after around 30 min of scanning. The normalized spectrum before scanning and after saturation is shown in Fig. 2. The high-extinction mode group we study in this Letter is the fundamental TE00 mode of the ring resonator with radius of 80 μm, which has a free spectral range (FSR) of 2.1 nm around 1550 nm and average loaded Q of 6×10^5. A universal blue shift of 0.76 nm is observed in the TE00 mode group. The saturation behavior can be explained by the limited defect density available for charge excitation and the trapping process in LN crystal [3,16]. The average loaded Q of the TE00 mode group remains approximately unchanged before and after the blue shift. We also record the time-dependent relaxation of resonances at 1.8 K. The TE00 mode group experiences a relaxation of 0.21 nm after four days, and a characteristic time constant of more than 10 days is obtained from exponential fitting of the recorded shift trace.

After saturation of the universal blue shift induced by repeated scanning, the TE00 mode at 1552.4 nm remains a Lorentzian shape when probed with a weak light (−25 dBm to the fridge), as shown in Fig. 3(a). Interestingly, after a strong light (5 dBm to the fridge) is launched into this mode, the resonance experiences a frequency shift, and the laser will be out of resonance in a few seconds. A mode splitting of the same mode could be observed in subsequent weak laser scan measurements [Fig. 3(b)]. This mode splitting of several resonance linewidths is preserved for days in the absence of further strong light illumination, indicating its origin from the long-lived space-charge field induced by the PR effect. This mode splitting of single resonance is attributed to the back scattering between the clockwise (CW) and counter clockwise (CCW) modes, which are renormalized into two standing-wave modes of different frequencies $\omega_0 \pm g$. Here ω_0 is the original frequency of the resonance mode m_0, and g describes the coupling strength between CW and CCW modes. In a microring/microdisk cavity, this back scattering is normally contributed by the roughness of the cavity surface [26]. We found that the PR-effect-induced mode splitting is selective and not universal. It is resolved only in TE00 modes with azimuthal mode numbers close to the imprinted mode. The imprinted TE00 mode at 1552.4 nm has an azimuthal mode number of $m_0 \approx 740$. As shown in Fig. 3, after the imprint process, the largest mode splitting occurs in modes m_0 and $m_0 \pm 1$. As the azimuthal mode number

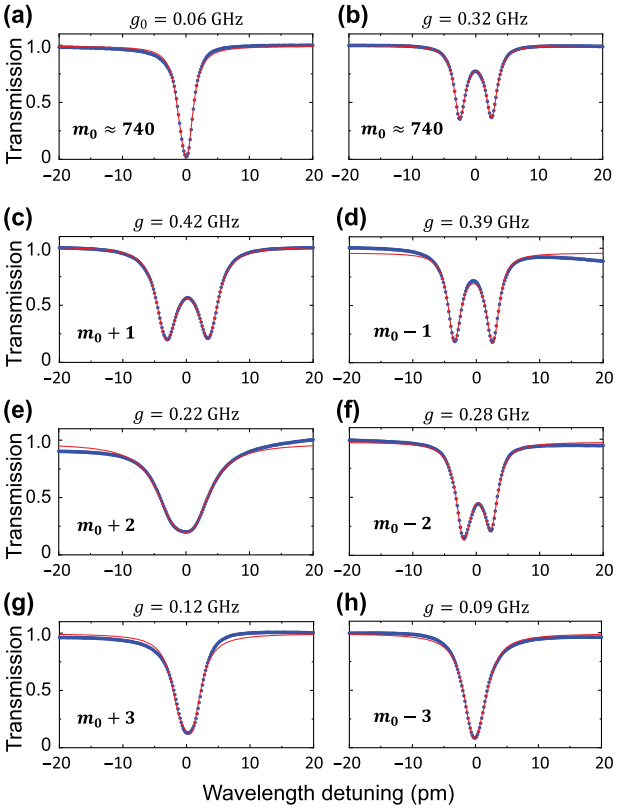

Fig. 3. PR-induced mode splitting measured after strong illumination of the selected TE00 mode at 1552.4 nm, with azimuthal mode number of $m_0 \approx 740$ in the 80 μm radius ring. Transmission spectrum of mode m_0 (a) before and (b) after strong light illumination. The fitted g_0 in (a) suggests a weak intrinsic back scattering in the ring resonator. (c)–(h) Transmission spectra of neighboring modes with azimuthal mode numbers $m_0 \pm 1$, $m_0 \pm 2$, and $m_0 \pm 3$ after strong light illumination. The fitted back-scattering strength g is indicated in each figure.

difference increases, the mode splitting becomes weaker, and indistinguishable when the modes are more then three FSRs away from the imprinted mode.

In the following, we present a theoretical description of the mode splitting process. Prior to the strong illumination of the selected cavity mode, an intrinsic weak Rayleigh back scattering already exists in the ring cavity due to surface roughness and inevitable fabrication imperfections [26,27]. When a strong light is launched in the microring, both CW and CCW traveling-wave modes are excited due to this intrinsic Rayleigh scattering. The cavity field can be expressed as

$$A(r, z, \phi) = A_{\mathrm{ccw}}(r, z)\Phi_{m_0}(\phi) + A_{\mathrm{cw}}(r, z)\Phi_{m_0}(-\phi), \quad \textbf{(1)}$$

where A_{cw} and A_{ccw} represent the amplitudes of CW and CCW imprint modes initially set by the launched and back-scattered light; m_0 is the azimuthal mode number of the imprint mode. Due to broken rotation symmetry in x-cut LN, $\Phi_m(\phi) \simeq \exp(i(m\phi - f\sin(2\phi)))$, where $f \simeq \pi R(n_o - n_e)/2\lambda$ is determined by ring radius R [28]. For simplification, we set the initial phase to be zero without loss of generality in the derivation. The optical field intensity I is proportional to $|A|^2$, and therefore introduces a ϕ-dependent standing-wave term, $I_{\mathrm{sw}}(\phi) \propto 2|A_{\mathrm{ccw}}A_{\mathrm{cw}}|\Re[\Phi^2_{m_0}(\phi)]$.

We assume the photovoltaic effect will build up a space-charge field in proportion to the imprint light intensity along crystalline z direction of [16]; thus, the ϕ-dependent space-charge field on the cavity should satisfy $E_{\mathrm{sc}}(\phi) = E_{\mathrm{sc},0}\Re[\Phi^2_{m_0}(\phi)]$. Considering the crystalline direction of x-cut LN film, the ϕ-dependent refractive index modulation that induces non-universal mode splitting can be calculated:

$$\delta n(\phi) \approx \frac{E_{sc,0}}{4n_{\mathrm{eff}}}\Re[(r_{33} + r_{13})\Phi^2_{m_0}(\phi) + \frac{(r_{33} - r_{13})}{2}(\Phi^2_{m_0-1}(\phi) + \Phi^2_{m_0+1}(\phi))], \quad \textbf{(2)}$$

where $n_{\mathrm{eff}} = [2n_o^2 n_e^2/(n_o^2 + n_e^2)]^{1/2}$ is the effective index of the LN ring cavity, and r_{13} and r_{33} are the electro-optic coefficients of LN. The PR-induced back-scattering strength g of mth azimuthal mode is given by the integration of CW-CCW modal overlap weighted by the index modulation pattern, and the result can be simplified to

$$g = \frac{\omega}{2n\pi}\int \delta n(\phi)\Phi^2_{m_0}(\phi)\mathrm{d}\phi, \quad \textbf{(3)}$$

where ω is the resonance frequency. The value of g can be derived with Eqs. (2) and (3):

$$g = \begin{cases} \frac{(r_{33}+r_{31})\omega E_{\mathrm{sc},0}}{8n^2_{\mathrm{eff}}} & m = m_0, \\ \frac{(r_{33}-r_{31})\omega E_{\mathrm{sc},0}}{16n^2_{\mathrm{eff}}} & m = m_0 \pm 1, \\ 0 & m \neq m_0, m_0 \pm 1, \end{cases} \quad \textbf{(4)}$$

which theoretically predicts non-zero back-scattering strength g for modes $m = m_0$ and $m = m_0 \pm 1$, and the mode splitting value of mode m_0 should be higher than the value of mode $m_0 \pm 1$. In the experiment, the mode splitting of mode $m_0 \pm 1$ is comparable to mode m_0, and also splitting for mode $m_0 \pm 2$ is observed. This deviation between theoretical prediction and experimental data suggests that the imprinted pattern is not perfectly matched with our prediction. The intrinsic roughness of the probed cavity mode, which is ignored in Eq. (2), could also contribute to the back-scattering process. The presence of a bus waveguide and the second ring also breaks the rotational symmetry, leading to imperfections with Fourier components having 180° and 90° periodicity. Furthermore, our simple model only linearly relates the index pattern to the local optical intensity. Although it captures some of the features of the PR-induced mode splitting, further investigation is needed to understand the detailed space-charge generation and photon-trap coupling dynamics. A full-fledged model should also consider the microscopic spatial charge distribution both longitudinal and transverse to the waveguides and self-consistently solve for the space field and corresponding index modulation. We anticipate a z-cut single-ring resonator will provide better symmetry and exhibit more distinctive mode-splitting features.

The imprinted index pattern can be redistributed by shifting the strong excitation to other modes, thus selectively inducing splitting in other modes at different wavelengths. A demonstration of this reconfiguration process is shown in Fig. 4. An initial index pattern is imprinted by launching strong light (5 dBm to fridge) into mode A at 1552.4 nm, introducing a mode splitting on this mode. By periodically scanning the laser wavelength from 1500 to 1600 nm covering 50 FSR with an input power of

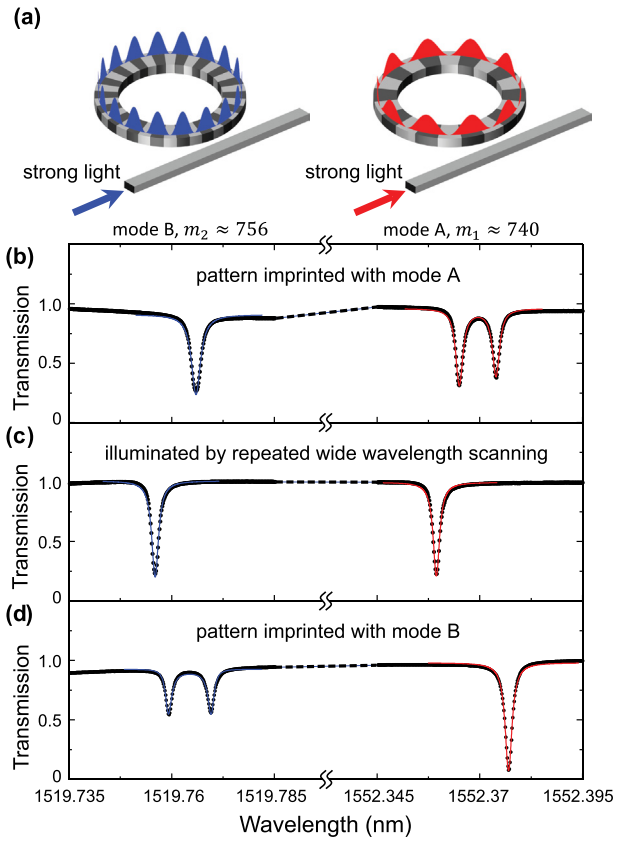

Fig. 4. (a) Schematic illustration of space-charge redistribution by strongly exciting different azimuthal modes. (b)–(d) Transmission spectrum measured by a weak probe light during the reconfiguration sequence. (b) Mode splitting around of TE00 mode A at 1552.4 nm is first generated by launching strong light into mode A. (c) Mode splitting vanishes after the device is uniformly illuminated by repeated broadband laser scanning from 1500 to 1600 nm. (d) A strong light is re-launched into mode B at 1519.7 nm, reconfiguring the mode splitting to mode B.

5 dBm for several times, the space charge is smoothed out and mode splitting vanishes. A strong pump light is then launched into mode B at 1519.76 nm, 16 FSR away from mode A. As shown in Fig. 4(d), the mode splitting is then reconfigured to mode B, while the original mode A around 1552.4 nm remains unchanged. Here we demonstrate that the information of mode splitting could be written and erased through strong imprint light and read by weak probe light. This reconfigurable feature of the PR effect at a low temperature shows a potential that could be utilized as optically addressable switching or reconfigurable photonic components.

In conclusion, due to the extremely long relaxation time of the PR-induced space charges at cryogenic temperatures, the PR effect presents a significant challenge in nonlinear LN photonic devices that require strong optical pumping such as quantum frequency converters and microwave-to-optical converters. With active manipulation of the pump light, the space charges can be redistributed at much faster time scales for active manipulation of target optical modes. In particular, we show that by intensively illuminating the device, a periodic refractive index grating can be configured and read out with a subsequent weak probe light. The device we characterized therefore possesses memory and reconfiguration capabilities that could be potentially utilized for on-chip all-optical reconfigurable photonic components.

Funding. U.S. Department of Energy (DE-SC0019406); David and Lucile Packard Foundation; National Science Foundation (EFMA-1640959); Army Research Office (911NF-18-1-0020, W911NF-19-2-0115).

Acknowledgment. The authors thanks Michael Rooks, Yong Sun, Sean Rinehart, and Kelly Woods for support in the cleanroom and assistance with device fabrication. HXT acknowledges partial support from NSF, ARO, and the Packard Foundation. Funding for substrate materials used in this research was provided by DOE/BES.

Disclosures. The authors declare no conflicts of interest.

REFERENCES

1. L. Arizmendi, Phys. Status Solidi A **201**, 253 (2004).
2. R. Weis and T. Gaylord, Appl. Phys. A **37**, 191 (1985).
3. T. Hall, R. Jaura, L. Connors, and P. Foote, Prog. Quantum Electron. **10**, 77 (1985).
4. D. Von der Linde, O. Schirmer, and H. Kurz, Appl. Phys. **15**, 153 (1978).
5. T. Volk, N. Rubinina, and M. Wöhlecke, J. Opt. Soc. Am. B **11**, 1681 (1994).
6. Y. Kong, S. Liu, and J. Xu, Materials **5**, 1954 (2012).
7. J. Lu, J. B. Surya, X. Liu, A. W. Bruch, Z. Gong, Y. Xu, and H. X. Tang, Optica **6**, 1455 (2019).
8. Y. Guo, Y. Liao, L. Cao, G. Liu, Q. He, and G. Jin, Opt. Express **12**, 5556 (2004).
9. A. Yariv, S. S. Orlov, and G. A. Rakuljic, J. Opt. Soc. Am. B **13**, 2513 (1996).
10. M. Bazzan and C. Sada, Appl. Phys. Rev. **2**, 040603 (2015).
11. M. Zhang, C. Wang, R. Cheng, A. Shams-Ansari, and M. Lončar, Optica **4**, 1536 (2017).
12. Z. Gong, X. Liu, Y. Xu, M. Xu, J. B. Surya, J. Lu, A. Bruch, C. Zou, and H. X. Tang, Opt. Lett. **44**, 3182 (2019).
13. C. Wang, M. Zhang, M. Yu, R. Zhu, H. Hu, and M. Loncar, Nat. Commun. **10**, 1 (2019).
14. C. Wang, X. Xiong, N. Andrade, V. Venkataraman, X.-F. Ren, G.-C. Guo, and M. Lončar, Opt. Express **25**, 6963 (2017).
15. Y. He, Q.-F. Yang, J. Ling, R. Luo, H. Liang, M. Li, B. Shen, H. Wang, K. Vahala, and Q. Lin, Optica **6**, 1138 (2019).
16. X. Sun, H. Liang, R. Luo, W. C. Jiang, X.-C. Zhang, and Q. Lin, Opt. Express **25**, 13504 (2017).
17. H. Jiang, R. Luo, H. Liang, X. Chen, Y. Chen, and Q. Lin, Opt. Lett. **42**, 3267 (2017).
18. H. Liang, R. Luo, Y. He, H. Jiang, and Q. Lin, Optica **4**, 1251 (2017).
19. M. Li, H. Liang, R. Luo, Y. He, J. Ling, and Q. Lin, Optica **6**, 860 (2019).
20. M. Soltani, M. Zhang, C. Ryan, G. J. Ribeill, C. Wang, and M. Loncar, Phys. Rev. A **96**, 043808 (2017).
21. T. P. McKenna, J. D. Witmer, R. N. Patel, W. Jiang, R. Van Laer, P. Arrangoiz-Arriola, E. A. Wollack, J. F. Herrmann, and A. H. Safavi-Naeini, "Cryogenic microwave-to-optical conversion using a triply-resonant lithium niobate on sapphire transducer," arXiv:2005.00897 (2020).
22. L. Shao, N. Sinclair, J. Leatham, Y. Hu, M. Yu, T. Turpin, D. Crowe, and M. Loncar, "Integrated microwave acousto-optic frequency shifter on thin-film lithium niobate," arXiv:2005.03794 (2020).
23. A. Youssefi, I. Shomroni, Y. J. Joshi, N. Bernier, A. Lukashchuk, P. Uhrich, L. Qiu, and T. J. Kippenberg, "Cryogenic electro-optic interconnect for superconducting devices," arXiv:2004.04705 (2020).
24. X. Lu, S. Rogers, W. C. Jiang, and Q. Lin, Appl. Phys. Lett. **105**, 151104 (2014).
25. J. Lu, J. B. Surya, X. Liu, Y. Xu, and H. X. Tang, Opt. Lett. **44**, 1492 (2019).
26. K. Iwatsuki, K. Hotate, and M. Higashiguchi, Appl. Opt. **23**, 3916 (1984).
27. M. Borselli, T. J. Johnson, and O. Painter, Opt. Express **13**, 1515 (2005).
28. J. Fürst, B. Sturman, K. Buse, and I. Breunig, Opt. Express **24**, 20143 (2016).